

# Diffuse reflectance of oceanic waters.

## III. Implication of bidirectionality for the remote-sensing problem

André Morel and Bernard Gentili

The upwelling radiance field beneath the ocean surface and the emerging radiance field are not generally isotropic. Their bidirectional structure depends on the illumination conditions (the Sun's position in particular) and on the optical properties of the water body. In oceanic case 1 waters, these properties can be related, for each wavelength  $\lambda$ , to the chlorophyll (Chl) concentration. We aim to quantify systematically the variations of spectral radiances that emerge from an ocean with varying Chl when we change the geometric conditions, namely, the zenith–Sun angle, the viewing angle, and the azimuth difference between the solar and observational vertical planes. The consequences of these important variations on the interpretation of marine signals, as detected by a satelliteborne ocean color sensor, are analyzed. In particular, the derivation of radiometric quantities, such as  $R(\lambda)$ , the spectral reflectance, or  $[L_w(\lambda)]_N$ , the normalized water-leaving radiance that is free from directional effects, is examined, as well as the retrieval of Chl. We propose a practical method that is based on the use of precomputed lookup tables to provide values of the  $f/Q$  ratio in all the necessary conditions [ $f$  relates  $R(\lambda)$  to the backscattering and absorption coefficients, whereas  $Q$  is the ratio of upwelling irradiance to any upwelling radiance]. The  $f/Q$  ratio, besides being dependent on the geometric configuration (the three angles mentioned above), also varies with  $\lambda$  and with the bio-optical state, conveniently depicted by Chl. Because Chl is one of the entries for the lookup table, it has to be derived at the beginning of the process, before the radiometric quantities  $R(\lambda)$  or  $[L_w(\lambda)]_N$  can be produced. The determination of Chl can be made through an iterative process, computationally fast, using the information at two wavelengths. In this attempt to remove the bidirectional effect, the commonly accepted view relative to the data-processing strategy is somewhat modified, i.e., reversed, as the Chl index becomes a prerequisite parameter that must be identified prior to the derivation of the fundamental radiometric quantities at all wavelengths. © 1996 Optical Society of America

### 1. Introduction

By simulating the radiation transport within the ocean–atmosphere system with a Monte Carlo code, it has been shown that the upward radiance field just beneath the ocean surface and therefore the field of the radiances leaving the ocean are in most cases anisotropic (Morel and Gentili<sup>1</sup>). In essence, this anisotropy results from the anisotropic optical properties of the water body (namely, its volume scattering function) combined with the illumination conditions that

prevail above the surface. These conditions are determined by the position of the Sun and the relative proportions of direct (Sun) and diffuse (sky) radiations.

Evidence has been presented (Morel *et al.*<sup>2</sup>) in favor of the previous theoretical results<sup>1</sup> through a comparison with field determinations using a submersible camera system, recently developed by Voss,<sup>3</sup> which allows the upwelling radiance distribution to be determined at several wavelengths. The practical consequences of these findings after interpretation of the marine signal, as detected by a satelliteborne ocean color sensor, are not yet fully analyzed, even if a first insight into this problem was gained thanks to the previous study (see Fig. 10 in Morel and Gentili<sup>1</sup>).

Our aim is to quantify systematically the variations of the spectral radiances that emerge from the ocean,  $L_w(\lambda)$ , for various oceanic waters (with varying chlorophyll content), when we change the geometric configuration, namely, the zenith observation angle

---

The authors are with the Laboratoire de Physique et Chimie Marines, Université Pierre et Marie Curie et Centre National de la Recherche Scientifique, Boite postale 8, F 06230 Villefranche-sur-mer, France.

Received 9 October 1995; revised manuscript received 6 March 1996.

0003-6935/96/244850-13\$10.00/0

© 1996 Optical Society of America

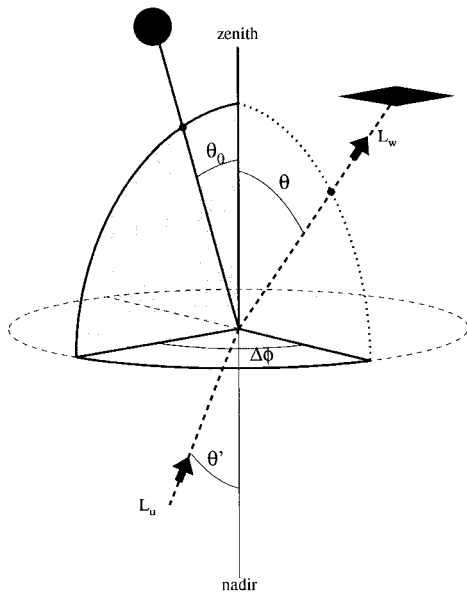


Fig. 1. Schematic geometry and symbols for radiances and angles. Note that  $\theta$  is a zenith angle and  $\theta'$  is a nadir angle.

( $\theta$ ), the zenith Sun angle ( $\theta_0$ ), and the azimuth difference ( $\Delta\phi$ ) between the solar and observation vertical planes; see Fig. 1. The geometric configurations to be examined in particular are those typical of a Sun-synchronous orbiting instrument; the wavelengths ( $\lambda$ ) considered are those used for the quantitative detection of constituents optically active in the visible part of the spectrum, such as chlorophyll, taken as an example of major interest. The various oceans considered are assumed to be homogeneous, with optical properties and chlorophyll concentration uniformly distributed along the vertical within the upper layers.

The bias introduced into the chlorophyll  $a$  concentration retrieval, when the angular variations of  $L_w(\lambda)$  are ignored, is assessed as an error budget when we operate the appropriate algorithms. Only algorithms that apply to the marine signals are considered. In other words, the estimate of the atmospheric contribution to the total radiance recorded by the sensor is supposed to be achievable and actually achieved in an independent way so that, by subtraction, the marine signals have already been accurately extracted from the total signal. At least in principle and owing to a set of near-IR channels, this independence is ensured with the new sensors such as sea-viewing wide field-of-view sensor (SeaWiFS), ocean color and temperature scanner, polarization and directionality of the Earth's reflectances, medium resolution imaging spectrometer, and moderate resolution imaging spectrometer. The signals from these channels can be used for the assessment of the atmospheric contribution, hereafter extrapolated as an atmospheric correction toward the visible part of the spectrum.

The situation with the defunct Coastal Zone Color Scanner (CZCS) was less comfortable because only one channel (at 670 nm) was available for estimating the aerosol contribution. Therefore hypotheses or addi-

tional information were needed to establish an atmospheric correction scheme. Such information was sought for in other (visible) channels, in which the atmospheric and marine signals actually intermingle. The solution was in the adoption of assumptions concerning the water-leaving radiances from selected pixels (the clearest pixels in the method proposed by Gordon and Clark<sup>4</sup>) or in the development of iterative schemes (in the method proposed by Bricaud and Morel<sup>5</sup> and by André and Morel<sup>6</sup>), through which the marine algorithms and atmospheric correction algorithms were no longer independent. Introducing the angular dependencies of the  $L_w$ 's within such iterative computations results in simultaneous changes in both the atmospheric correction and the chlorophyll  $a$  retrieval. This rather complex situation, typical of the CZCS, was examined elsewhere (Myrmehl and Morel<sup>7</sup>), and the consequence of ignoring the angular variations of  $L_w$  was analyzed and quantified in terms of chlorophyll  $a$  concentration deviation. This particular case is not reexamined in this study.

## 2. Theoretical Background

### A. Basic Equations

The wavelength dependence is not made explicit except when needed for clarity. If  $L_u(0^-, \theta', \phi)$  represents the upward radiance beneath the ocean surface (at null depth, denoted  $0^-$ ), the radiance transmitted through the interface that then emerges from the ocean [the water-leaving radiance,  $L_w(\theta, \phi)$ ] can be expressed as (e.g., Gordon and Morel<sup>8</sup>)

$$L_w(\theta, \phi) = L_u(0^-, \theta', \phi) \frac{[1 - \rho(\theta', \theta)]}{n^2}, \quad (1)$$

where (see Fig. 1)  $\phi$  is the azimuth angle,  $\theta$  is the zenith angle (in air),  $\theta'$  is the corresponding refracted nadir angle (in water), with  $\theta' = \sin^{-1}(\sin \theta/n)$ ,  $\rho(\theta', \theta)$  is the internal Fresnel reflectance for the associated directions ( $\theta', \theta$ ), and  $n (= 1.34)$  is the refractive index of water. The fraction of the downward radiant flux that enters the ocean surface and is then returned upward is represented by

$$R(0^-) = \frac{E_u(0^-)}{E_d(0^-)}, \quad (2)$$

where  $R(0^-)$  is the reflectance or irradiance ratio at null depth and  $E_d$  and  $E_u$  are the downward and upward irradiances, respectively. These are the integrals of the radiance fields when weighted by the cosine of the incident angles over the upper hemisphere  $\Xi_d$  (downward directions,  $0 < \theta < \pi/2$ ) and lower hemisphere  $\Xi_u$  (upward directions,  $0 < \theta' < \pi/2$ ) and when  $\phi$  varies between 0 and  $2\pi$ :

$$E_d(0^-) = \int_{\Xi_d} L_d(0^-, \theta, \phi) \cos \theta d\Omega, \quad (3a)$$

$$E_u(0^-) = \int_{\Xi_u} L_u(0^-, \theta', \phi) \cos \theta' d\Omega, \quad (3b)$$

where  $d\Omega$  is the differential element of a solid angle. The reflectance ratio depends on the zenith Sun angle  $\theta_0$  (see below) and is thereafter noted as  $R(\theta_0)$ . The  $Q$  function (in units of steradians) is defined as the ratio of irradiance to any radiance (both at  $0^-$ ),

$$Q = E_u(0^-)/L_u(0^-, \theta', \phi),$$

and would be  $\pi$  if the  $L_u$  distribution were isotropic. This  $Q$  function is actually a bidirectional function to the extent that  $L_u$  depends on the direction from which it originates and also on the illumination conditions and then on  $\theta_0$  and on  $\Delta\phi$ , the azimuth difference (Fig. 1). Therefore  $Q$  is a function of three angles according to (argument  $0^-$  omitted)

$$Q(\theta', \theta_0, \Delta\phi) = E_u/L_u(\theta', \theta_0, \Delta\phi). \quad (4)$$

By using Eqs. (1), (2), and (4) and taking into account the downward, internal reflection at the interface, we obtain

$$L_w(\theta, \theta_0, \Delta\phi) = \frac{E_d(0^-)[1 - \rho(\theta', \theta)]}{(1 - \bar{r}R)n^2} \frac{R(\theta_0)}{Q(\theta', \theta_0, \Delta\phi)},$$

where  $\bar{r}$ , the water-air Fresnel reflection for the whole diffuse upwelling irradiance, is of the order of 0.48.<sup>9</sup> If the downwelling irradiance above the ocean surface,  $E_d(0^+)$ , replaces  $E_d(0^-)$ , we obtain

$$L_w(\theta, \theta_0, \Delta\phi) = E_d(0^+) \times \left\{ \frac{(1 - \bar{\rho})[1 - \rho(\theta', \theta)]}{(1 - \bar{r}R)n^2} \right\} \frac{R(\theta_0)}{Q(\theta', \theta_0, \Delta\phi)}, \quad (5)$$

where  $\bar{\rho}$ , the air-water Fresnel reflection at the interface for the whole (Sun + sky) downwelling irradiance, typically amounts to between 4% and 5%. The fraction within braces will be replaced by  $\mathfrak{R}(\theta)$ , a term that merges all the reflection and refraction effects and depends essentially on  $\theta$ , through  $\rho(\theta', \theta)$ , and therefore on the sea state (Fig. 11), and weakly on  $\theta_0$ . The downwelling irradiance above the air-sea interface,  $E_d(0^+)$ , can be expressed as a function of the mean extraterrestrial solar irradiance  $F_0$  after one has taken into account the Sun angle (through  $\mu_0 = \cos \theta_0$ ), the atmospheric diffuse transmittance [through  $t(\theta_0)$ ], and the varying Sun-Earth distance that is due to the ellipticity of the Earth's orbit; the last effect is expressed through the parameter  $\varepsilon = (\bar{d}/d)^2$ , where  $\bar{d}$  and  $d$  are the mean and actual Earth-Sun distances, respectively.

By introducing these parameters, Eq. (5) can be rewritten as

$$L_w(\theta, \theta_0, \Delta\phi) = [F_0 \varepsilon t(\theta_0) \mu_0] \mathfrak{R}(\theta) \frac{R(\theta_0)}{Q(\theta', \theta_0, \Delta\phi)}. \quad (6)$$

According to Gordon and Clark,<sup>4</sup> the normalized water-leaving radiance,  $(L_w)_N$ , was defined as the radiance that could be measured by a nadir-viewing instrument, if the Sun were at the zenith in the absence of any atmospheric loss, and when the Earth is

at its mean distance from the Sun. From this definition it follows that, when aiming at nadir,  $\theta' = \theta = 0$  (thus  $\phi$  is undetermined), and  $L_w(\theta, \theta_0, \Delta\phi)$  reduces to  $L_w(0, 0)$ ; for normal incidence  $\rho(0)$  is minimal (0.021) and  $\mathfrak{R}(\theta)$  has a maximal value of  $\mathfrak{R}_0 = 0.529$  (see Appendix D); finally  $Q(\theta', \theta_0, \Delta\phi)$  also reduces to  $Q(0, 0)$ , hereafter denoted as  $Q_0$ , and  $R$  (when  $\theta_0 = 0$ ) is denoted as  $R_0$ . By introducing these modifications and appropriate notations, Eq. (6), when written for  $(L_w)_N$ , becomes

$$(L_w)_N = \frac{F_0 \mathfrak{R}_0}{Q_0} R_0, \quad (7)$$

which conforms exactly to the requirements of the normalized water-leaving radiance definition. Operational definitions of  $(L_w)_N$  also exist and are in current use despite their imprecise character (see Appendix A). By keeping the exact definition above,<sup>4</sup> any slant water-leaving radiance can be expressed as a function of  $(L_w)_N$  according to

$$L_w(\theta, \theta_0, \Delta\phi) = [\varepsilon t(\theta_0) \mu_0] \frac{R(\theta_0) \mathfrak{R}(\theta)}{R_0 \mathfrak{R}_0} \frac{Q_0}{Q(\theta', \theta_0, \Delta\phi)} (L_w)_N. \quad (8)$$

Differing from the reflectance defined by Eq. (2), the remote-sensing (RS) reflectance,  $R_{RS}$ , introduced by Carder and Steward,<sup>10</sup> is sometimes used (see, e.g., Lee *et al.*<sup>11</sup>); it represents the ratio of the vertically emerging radiance to the above-surface downwelling irradiance (see Appendix B).

## B. Accounting for all Variables

The illumination conditions that are determined mainly by the position of the Sun, also vary with atmospheric turbidity ( $\tau_a$ , the aerosol optical depth), which governs the direct and diffuse contributions to the total incident radiation just above the surface. Therefore  $Q$  is also a function of  $\tau_a$ . In addition, given the position of the Sun and  $\tau_a$ , the geometric structure of the entering downward stream and subsequently the  $L_u$  field created by backscattering from this stream are influenced by the characteristics of a wavy interface. As a consequence the  $Q$  function is, at least in principle, sensitive to the wave slopes. They can be related to the wind speed ( $W$ ) so that  $W$  would be an additional variable.

Since the geometric conditions of illumination are fixed, the structure of the  $Q$  function depends on the inherent optical properties of the water body,<sup>1</sup> namely, on  $\bar{\omega}$ , the single-scattering albedo of the water, and on  $\eta_b$ , the ratio of water molecular backscattering to the total (molecules plus particles) backscattering coefficient. Finally, when we take into account the above variables, the  $Q$  function can be written as

$$Q[\theta', \theta_0, \Delta\phi, \tau, W, \bar{\omega}(\lambda), \eta_b(\lambda)] \quad (9a)$$

or

$$Q_n[\theta_0, \Delta\phi, \tau, W, \bar{\omega}(\lambda), \eta_b(\lambda)] \quad (9b)$$

or also

$$Q_0[\tau, W, \bar{\omega}(\lambda), \eta_b(\lambda)]. \quad (9c)$$

The first expression is the most general, whereas the second applies to the particular case of upward radiance that originates from nadir (subscript  $n$ , when  $\theta' = 0$ ) and the third is  $Q_n$  when  $\theta_0 = 0$  [as in Eq. (7)]. In expressions (9a)–(9c) the wavelength dependency of  $\bar{\omega}$  and  $\eta_b$  is made explicit. For oceanic case 1 waters, these spectrally variable parameters are actually governed by the pigment concentration (Figs. 2 and 3 in Ref. 1), so that  $\bar{\omega}$  and  $\eta_b$  can simply be replaced by  $\lambda$  and Chl when needed; Chl represents the chlorophyll concentration expressed in  $\text{mg m}^{-3}$ . Indeed, there is a simplifying assumption in the above presentation and in expressions (9a)–(9c). The use of only two parameters,  $\bar{\omega}$  and  $\eta_b$ , hereafter replaced by  $\lambda$  and Chl, for characterizing a water body implies that a unique volume scattering function (VSF) for marine particles has been adopted. Under this proviso, the shape of the VSF for any water body can be fully determined by  $\eta$ , the ratio of molecular scattering to total (molecules plus particles) scattering;  $\eta_b$  is also univocally related to  $\eta$  (Fig. 5 in Ref. 12). There is evidence that the particle VSF is not constant in shape and the above assumption, as already noted,<sup>1</sup> results in a limitation of the Chl range that can be reliably considered.<sup>13</sup>

Three plots of  $Q_n(\theta_0)$  for  $\theta_0 = 15^\circ, 30^\circ$ , and  $60^\circ$  as a function of  $\lambda$  and of Chl were displayed in Ref. 1 (Fig. 13). It has also been shown [Fig. 9(a) in Ref. 1] that  $Q$  may vary between approximately 3.1 and 5.6 when the directions considered ( $\theta', \Delta\phi$ ) are those involved in the remote-sensing (RS) configuration (with  $\theta$  limited to  $50^\circ$ , then  $0 < \theta' < 35^\circ$ ) and when  $\theta_0$  varies from  $0$  to  $80^\circ$ . In these simulations the wavelengths (440, 500, 565, and 665 nm) were typical of an ocean color sensor, and Chl was increased from  $0.03$  to  $3 \text{ mg m}^{-3}$ . The wind speed ( $2 \text{ ms}^{-1}$ ) and the aerosol load corresponding to a horizontal visibility of  $23 \text{ km}$  were not varied in these simulations.

### C. Diffuse Reflectance and Inherent Properties

The dimensionless quantity  $R$  can be related to the inherent optical properties of the water body, namely, to  $b_b$  and  $a$ , the backscattering and the absorption coefficients, according to

$$R = f \frac{b_b}{a} \quad (10a)$$

or

$$R = f' \frac{b_b}{a + b_b}. \quad (10b)$$

The structure of Eq. (10a) comes from Morel and Prieur<sup>14</sup>; when they developed a reflectance model,  $f$

was given the mean value of  $0.33$ . In Gordon *et al.*,<sup>15</sup>  $R$  was expressed as a power series of  $x [= b_b/(a + b_b)]$ , which can be simplified to Eq. (10b) with  $f'$  varying from  $0.324$  for a zenith Sun to  $0.369$  for a uniform sky.

As shown in Morel and Gentili,<sup>12</sup> the coefficient  $f$  is not constant and does vary in an orderly manner with the water optical properties (through  $\bar{\omega}$  and  $\eta_b$ ) and with the illumination conditions (through  $\theta_0$ ); a polynomial parameterization of  $f$  was proposed in Ref. 1. Actually the  $f$  or  $f'$  coefficients are similarly dependent on the same set of parameters according to

$$f[\theta_0, \tau, W, \bar{\omega}(\lambda), \eta_b(\lambda)],$$

and their variations are presented later. Again the possibility that the particle VSF may change is not accounted for in this approach. By merging Eqs. (5) and (10a) it follows that (simplified notation)

$$L_w(\theta, \theta_0, \Delta\phi) = E_a(0^+) \mathfrak{R}(\theta) \frac{f b_b}{Q a}, \quad (11)$$

or by reassembling Eqs. (7) and (10a) we obtain

$$(L_w)_N = F_0 \mathfrak{R}_0 \frac{f(0) b_b}{Q_0 a}. \quad (12)$$

For brevity, in Eqs. (11) and (12) we omit the set of parameters on which  $f$  and  $Q$  depend. Note that the ratio  $R(\theta_0)/R_0$  that appears in Eq. (8) or in Eq. (A3) in Appendix A actually reduces to the ratio of the corresponding  $f$  coefficients for  $\theta_0$  and for  $\theta_0 = 0$ .

### 3. Implication in the Remote-Sensing Problem

As mentioned in Section 1 we assume for what follows that the necessary atmospheric correction can be accurately applied to the signals recorded by the remote sensor in such a way that the spectral water-leaving radiances  $L_w(\theta, \Delta\phi, \lambda)$  are all available in the visible part of the spectrum. For analysis and interpretation of these marine signals, we can employ approaches ranging from totally empirical to fully analytical.<sup>16</sup> Here, only semianalytical models are considered, as represented by the ratios of optical properties that appear in Eqs. (10a) and (10b), where the partial contributions of the main optically active substances to the formation of the optical coefficients ( $a, b_b$ ) are parameterized. In case 1 waters,<sup>14,17</sup> these coefficients are (by definition) related only to the phytoplankton pigment concentration denoted Chl (and not  $C$ , which is the usual notation in the ocean color community).<sup>18</sup> To the extent that the ratio  $b_b(\lambda)/a(\lambda)$  can be derived from the measured radiances,  $L_w(\theta, \Delta\phi, \lambda)$ , the model can be inverted to retrieve Chl (see Appendix C).

Therefore, the first step consists of converting the  $L_w$ 's into the above ratios and such a conversion implies that the directional effects are taken into account and removed. In other words, the full dependencies of  $Q$  and  $f$  on geometry and water optical properties must be considered when one operates Eqs. (6) and (11). The model that involves the normalized water-

leaving radiance [Eqs. (7) and (12)] is identical to that which explicitly involves reflectance.

The relatively weak  $\mathfrak{R}(\theta)$  variations ruled by Fresnel reflection combined with the wave slopes are examined separately (Appendix D). Indeed, the major directional effect originates from the variations in the ratio  $f/Q$ , which are discussed after the variations of  $f$  and  $Q$  have been examined separately.

#### 4. Computational Aspects

The following results were obtained by operating a Monte Carlo model to simulate a coupled plane-parallel ocean-atmosphere system, including a wind-roughened interface (see the description in Ref. 19). Except if otherwise stated, the wind speed is set at zero for the routine computations and the optical thickness that is due to aerosol  $\tau_a$  is constant and equal to 0.20 at 550 nm. The atmosphere is modeled with 50, 1-km-thick layers as outlined by Elterman.<sup>20</sup> Tropospheric aerosol with a relative humidity of 70% and maritime aerosols with 90% relative humidity are located within the 45 upper layers or the lower five layers, respectively. Aerosol models and their phase functions were computed by Mie theory from the data of Shettle and Fenn.<sup>21</sup> The air-sea interface was modeled based on data from Cox and Munk<sup>22</sup> with a Gaussian distribution of surface slopes depending on wind speed  $W$ . For standard computations we set  $W$  equal to zero; note that residual capillary waves are still present in the absence of wind. Polarization is not accounted for in these simulations.

For the ocean, the dependence of the spectral inherent optical properties on the chlorophyll concentration is parameterized as in Fig. 6 in Ref. 1. The dependence of  $f$  and  $Q$  on  $\bar{\omega}$  and  $\eta_b$  is hereafter replaced by a dependence on the underlying variables  $\lambda$  and Chl. The relative contributions of molecular and particle scattering, each with its specific VSF, thus vary and depend only on  $\lambda$  and Chl. The wavelengths considered are 412, 443, 490, 510, 555 and 670 nm and the chlorophyll concentrations are 0.03, 0.1, 0.3, 1 and 3 mg m<sup>-3</sup>. However, because of the adoption of a unique VSF for marine particles, the simulation with 3 mg m<sup>-3</sup> of Chl remains questionable.<sup>13</sup> The Sun zenith angle was given the values 0, 15, 30, 45, 60, and 75°. The photons that travel upward were collected just beneath the surface into contiguous counters of variable solid angles and arranged according to constant increments in  $\Delta\phi$  (7.5°) and  $\theta'$  (5°). These counters provide the  $L_u(\theta_0, \theta', \Delta\phi)$  field at null depth and, by integrating, the upwelling irradiance  $E_u(0^-, \theta_0)$ . Other detectors are set to determine the downward field structure above the interface and inside the water body to a depth that is approximately equal to  $2.5/K_d$ . The final results of these simulations have been tabulated for subsequent interpolations; those shown in the following figures correspond to individual calculations and have not been interpolated.

Compared with previous Monte Carlo simulations,<sup>1</sup> the number of photon packets generated, or the actual number of collisions, has been increased by

a factor of at least 10 to reduce the stochastic noise. Even longer simulations, segmented into independent runs, have been effected for some specific cases; they have provided the possibility of studying the evolution of the means and standard deviations for the desired quantities and thus of optimizing the computation effort. As a result of the allowed computation time, the  $Q$  values were obtained with an accuracy (at  $1\sigma$ ) of  $\pm 2\%$  and the  $f$  values with an accuracy of better than 1%. In some particular cases, and for *a posteriori* verifications, duplicate computations have been carried out by using in parallel the much faster invariant embedding method developed by Mobley<sup>23</sup> (the HYDROLIGHT 3.0 code). The excellent agreement between the two sets of results (those provided by HYDROLIGHT are without statistical errors) demonstrates that the above-quoted accuracy is amply met.

#### 5. Results

The influence of  $\tau_a$  and wind speed are examined later as a sensitivity study. Considering simultaneously the effects of the five other variables ( $\theta_0$ ,  $\theta'$ ,  $\Delta\phi$ ,  $\lambda$ , Chl) can not be easily effected and the convenient way hereafter adopted consists of successively examining the behavior of  $f(\theta_0, \lambda, \text{Chl})$ , then that of  $Q_n(\theta_0, \lambda, \text{Chl})$ , as well as of their ratio. Finally some typical examples of the ratios  $f/Q$  for various viewing geometries, wavelengths, and chlorophyll concentrations are presented and discussed.

##### A. Evolution of $f(\theta_0)$

Examples of the variations in this factor with the zenith solar angle are displayed in Fig. 2. As already pointed out,<sup>12,24,25</sup>  $f(\theta_0)$  is minimal when  $\theta_0 = 0$  and always increases when  $\theta_0$  increases. For a given Sun angle and wavelength,  $f(\theta_0)$  is always higher if the chlorophyll concentration is higher. When  $\theta_0$  varies from 0 to 75°, the relative variation in  $f$  is enlarged for higher Chl, as a result of the enhanced role of particle scattering compared with that of molecular scattering.<sup>12</sup> For the same reason the  $f$  values appear to be more Chl dependent at 412 and 443 nm than they are at 670 nm, where the role of molecular scattering is always reduced. In summary, the  $f(0)$  values are all in the 0.29–0.33 range, and when one considers all the  $f(\theta_0)$  values, they are within the 0.29–0.48 interval with predictable evolutions.

##### B. Evolutions of the $Q_n$ Factor and the $f/Q_n$ Ratio

The  $Q_n(\theta_0, \lambda, \text{Chl})$  factor (Fig. 3), defined for nadir radiance ( $\theta' = 0$ ), is systematically minimal when  $\theta_0 = 0$ , with values (between approximately 3.2 and 3.9) ruled by increasing Chl. The strongest variations in  $Q_n$  with the Sun angle are observed for  $\lambda = 670$  nm, where  $\bar{\omega}$  is low enough so that single scattering predominates to form the upward flux.<sup>12</sup> Indeed, the average number of scattering events  $\bar{n}$  that the photons undergo before escaping is between 1.1 and 2.0 at this wavelength when Chl varies from 0.03 to 3 mg m<sup>-3</sup>. Even if the Chl value appears to be the governing factor rather than  $\lambda$ , the spectral pattern for

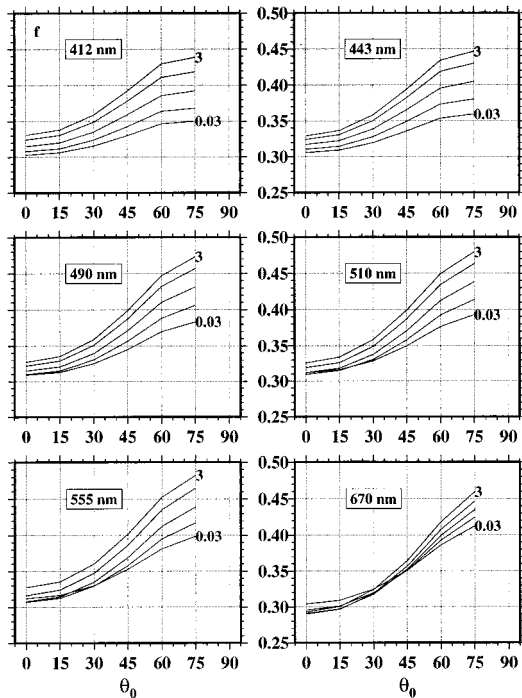


Fig. 2. Variations of  $f$  [Eq. (10a)] as a function of solar zenith angle  $\theta_0$  for various wavelengths and chlorophyll concentrations equal to 0.03, 0.1, 0.3, 1, and 3  $\text{mg m}^{-3}$  from bottom to top.

$Q_n$  (Fig. 4) is not neutral and exhibits reversed slopes for low and high solar elevations.

Because the  $f$  and  $Q_n$  quantities follow similar trends with changing Sun angle, the range of variation in their ratio between 0.095 and 0.075 is considerably reduced. The compensation is almost complete (Fig. 5) for the shortest wavelengths, whereas a residual, Chl-dependent, variation of  $f/Q_n$  with  $\theta_0$  subsists for larger wavelengths.

### C. Bidirectional Properties

To get a complete picture of the anisotropic upward radiant field, all the observation angles must be considered. Some examples of the variations in the ratio

$$f(\theta_0, \lambda, \text{Chl})/Q(\theta', \theta_0, \Delta\phi, \lambda, \text{Chl})$$

are displayed in Fig. 6. The strongest variations of this ratio are expected to occur in the principal plane that contains the Sun ( $\Delta\phi = 0$  or  $\pi$ ) and minimal variations are expected in the perpendicular plane ( $\Delta\phi = \pi/2$ , because of symmetry only the half-plane is shown in Fig. 6). When  $\Delta\phi$  changes between these extreme cases, the  $f/Q$  pattern evolves in a regular manner (not shown). Compared with Fig. 5, that deals with only vertically emerging radiances and in which  $f/Q_n$  was confined within a rather narrow interval, Fig. 6 shows that the  $f/Q$  ratio now undergoes large changes when all emerging radiances ( $\theta' \leq 48^\circ$ ) are considered, and considerable changes still subsist when only the  $\theta'$  angles involved in RS are considered ( $\theta' \leq 35^\circ$ ).

The general shape of these curves is dictated by

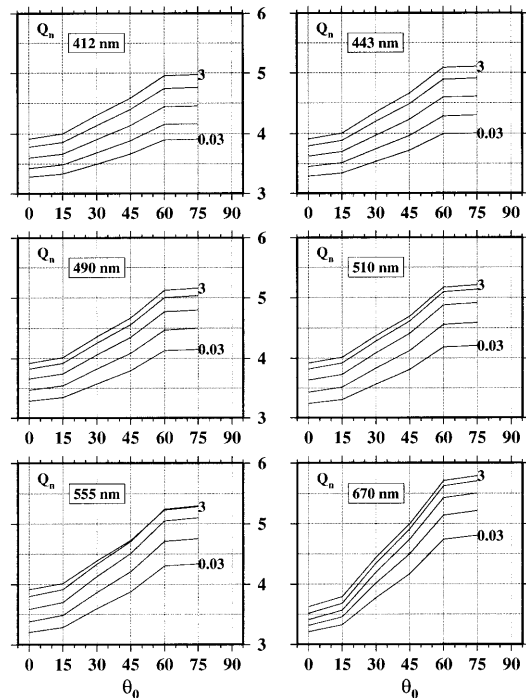


Fig. 3. For the wavelengths indicated, variation of  $Q_n$ , the specific value of the  $Q$  factor when the radiance originates from nadir, as a function of the solar zenith angle  $\theta_0$ . The various curves in each panel are for chlorophyll concentrations of 0.03, 0.1, 0.3, 1, and 3  $\text{mg m}^{-3}$  from bottom to top.

illumination conditions, and, for a given Sun angle, there is also a gradual transformation of the pattern with Chl. The larger amplitudes in  $f/Q$  are observed for chlorophyll-rich waters (as a result of the decreasing role of molecular scattering). The nonsymmetrical pattern (see, e.g., when  $\theta_0 = 75^\circ$ ) can be reversed from a low to a high chlorophyll concentration. Interestingly, the spectral dependency is reduced since the various curves remain close together whatever the wavelength (apart from 670 nm). This result is

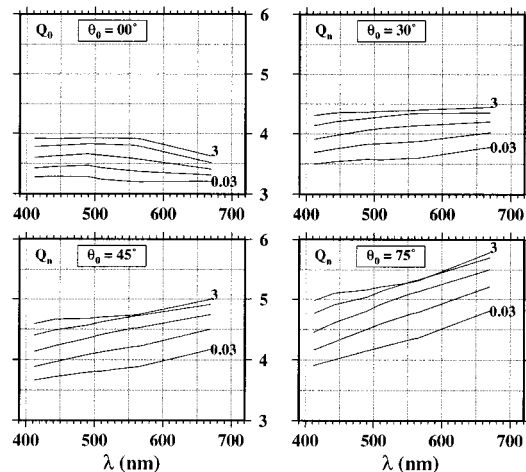


Fig. 4.  $Q_n$  plotted versus wavelength and for four specific values of  $\theta_0$ , as indicated. In the upper left panel where  $\theta_0 = 0^\circ$ ,  $Q_n$  has the specific value of  $Q_0$ .

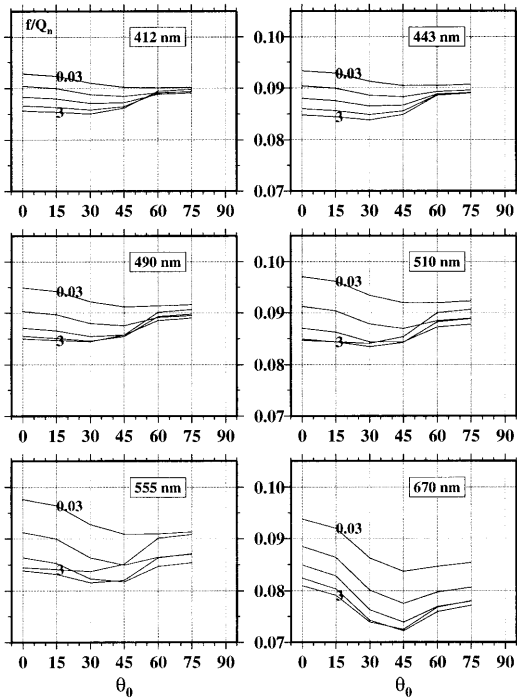


Fig. 5. Same as Figs. 2 and 3 except for the ratio  $f(\theta_0)/Q_n$ .

important from the perspective of one using ratios of radiances at two wavelengths, which appear to be much less sensitive to the viewing geometry than the individual radiances themselves.

Some specific features related to particle backscattering are visible, such as the relative weak maximum in  $f/Q$  at  $\theta' = 0$  (when  $\theta_0 = 0$ ) or at  $\theta' = -32^\circ$  (when  $\theta_0 = 45^\circ$ ), located in the opposite direction of the (refracted) Sun rays. Such peaks emerge only when single scattering predominates, as is the case at 670 nm. For shorter wavelengths,  $\bar{n}$  is always above 2 (double scattering) and reaches 5 or 6 for a chlorophyll level of  $1 \text{ mg m}^{-3}$ , so that these features related to the backscattering lobe vanish. In any case, they are questionable to the extent that the exact shape of the particle phase function for scattering angles near  $180^\circ$  is uncertain and actually has never been measured (but only extrapolated or computed by way of Mie theory and assumptions concerning the nature of suspended particles).

#### D. Practical Consequences

The curves displayed in Fig. 6 represent direct images of the  $L_w$  signals that would emerge from a uniform water body when observed from various  $\theta_0$  directions [Eq. (11)]. For a constant zenith Sun an-

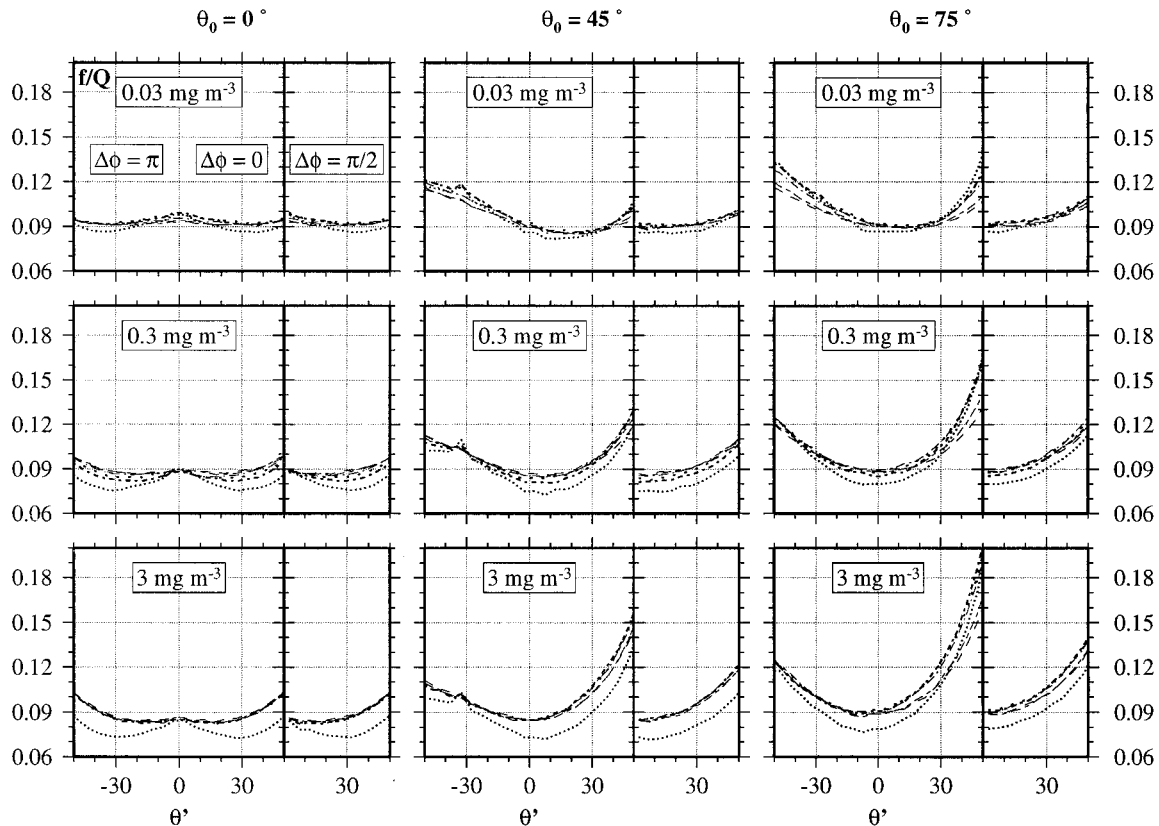


Fig. 6. Selected examples of the ratio  $f/Q$  for some  $\theta_0$  and Chl values as indicated and when  $\theta'$  varies from  $\pm 50^\circ$  with respect to the vertical direction and within the principal plane containing the Sun ( $\Delta\phi = 0$  or  $\pi$ ) or within the perpendicular half-plane ( $\Delta\phi = \pi/2$ ). The standard conditions for this figure are  $W = 0 \text{ ms}^{-1}$  and  $\tau_a = 0.20$ . Note that for RS applications and because of the sphericity of the Earth, a viewing angle  $\theta_v = 45^\circ$ , from an altitude of 705 km (SeaWiFS), corresponds to  $\theta = 52^\circ$  and  $\theta' = 36^\circ$ . With the scales adopted for these graphs, the curves corresponding to the various wavelengths are barely discernible except those for  $\lambda = 670 \text{ nm}$  (dotted curves). They are actually approximately arranged with increasing wavelength (410–670 nm) from top to bottom.

gle (a condition practically fulfilled within the swath of a Sun synchronous orbiting instrument), the possible variations in  $f/Q$ , and also in  $L_w$ , are increasingly important when Chl increases. In contrast to the  $\theta$ ,  $\theta_0$ , and  $\Delta\phi$  angles, Chl is obviously unknown when the processing of remotely sensed data is started, so that an iterative procedure appears inevitable, with the aim of progressively selecting the appropriate  $f/Q$  values. Such a technique is needed not only when trying to retrieve Chl but also, and more unexpectedly, when producing, from the measured  $L_w(\lambda)$ , any monochromatic radiometric quantity such as  $R(\lambda)$  or  $[L_w(\lambda)]_N$ . These two aspects are successively examined below.

#### E. Iterative Procedure to Retrieve Chlorophyll Concentration

When we initiate the processing, a simple method consists of selecting mean and constant values for  $f/Q$  at the two wavelengths ( $\lambda_1$  and  $\lambda_2$ ) of interest, if a ratio technique (such as the blue-to-green ratio; see Appendix C) is envisaged to assess chlorophyll. With these constant values, Eq. (11) can be inverted for each pixel of the scene and thus provides the ratios  $(b_b/a)$  at  $\lambda_1$  and  $\lambda_2$ . If we have at our disposal a bio-optical model with which  $(b_b/a)_{\lambda_1}/(b_b/a)_{\lambda_2}$  can be related to Chl, a first estimate of the concentration  $\text{Chl}_1$  can be derived. With  $\text{Chl}_1$  as the entry value, it becomes possible to enter into a table of  $f/Q$  and reprocess the data to obtain a second estimate, e.g.,  $\text{Chl}_2$ , and so forth.

An example of applying this procedure is shown in Fig. 7 for which we set up an arbitrary Chl distribution within the swath. In the simulation phase we computed the  $b_b/a$  ratios for two wavelengths (443 and 555 nm) from Chl and transformed them into the  $L_w$ 's by using Eq. (11) and the appropriate  $f/Q$  values (depending on  $\theta_0$ ,  $\Delta\phi$ ,  $\theta'$ , and Chl). These simulated  $L_w$ 's are those that could be derived from the sensor data after atmospheric correction is (perfectly) achieved. When we enter into the processing phase, the previous computation is to be ignored and values for  $f/Q$  at the two wavelengths can be arbitrarily adopted for a first step. The simplest way consists of assuming that these two values are constant whatever the position inside the swath (0.0936 and 0.0929 at 443 and 555 nm, respectively, according to the average values given in Ref. 1). The ratios of the  $(b_b/a)$  values at the two wavelengths were thus straightforwardly obtained [Eq. (11)] and then entered into the algorithm (Appendix C) to obtain a first guess of the chlorophyll content  $\text{Chl}_1$ . For the second iteration, we selected the proper  $f/Q$  values by using  $\text{Chl}_1$ ,  $\theta_0$ ,  $\theta'$ ,  $\Delta\phi$ , and the two  $\lambda$ 's as entries. Equation (11) can be solved again for  $b_b/a$  at these two wavelengths and second estimates  $\text{Chl}_2$  can be obtained. It is conceivable (and it has been checked) that other starting hypotheses (relative to the initial values adopted for  $f/Q$ ) have no impact on the final results after two or, at the most, three iterations.

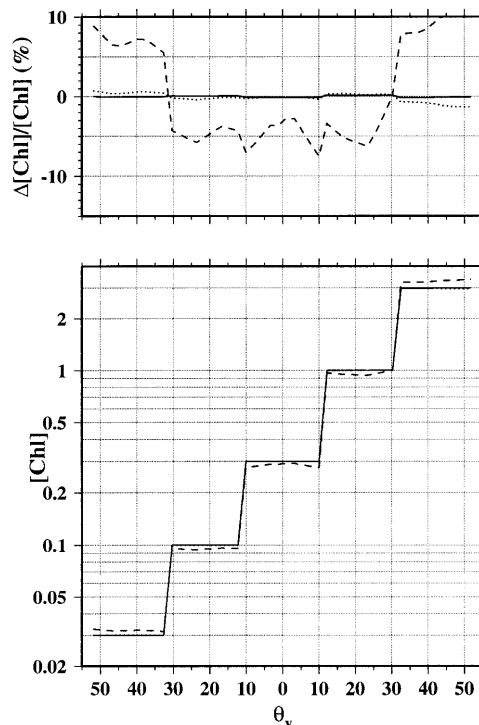


Fig. 7. Chlorophyll concentration (in  $\text{mg m}^{-3}$ , log scale) within a scan line of SeaWiFS (bottom, solid line). The geometric conditions are those of the SeaWiFS sensor, computed for the vernal Equinox (day 80) and for a subsatellite point on the polar arctic circle (in descending mode, noon orbit<sup>26</sup>);  $\theta_0$  is approximately  $65^\circ$  and  $\Delta\phi$  is between  $85^\circ$  and  $92^\circ$ , everywhere within the swath, and the swath corresponds to  $\theta = \pm 52^\circ$ . The dashed curve represents the retrieved  $\text{Chl}_1$  values after the first processing (see text). The relative error with respect to the input value (in percent) is also shown as a dashed curve in the upper panel; the dotted curve and solid line represent the relative errors after the first and second iterations, respectively.

#### F. Retrieving $(L_w)_N$ or $R$

In addition to simple ratio techniques, advanced algorithms that involve various combinations of several spectral channels are also envisaged for the retrieval of diverse substances (see, e.g., Refs. 11, 27, and 28). Therefore, at each wavelength, absolute values of  $R(\lambda)$  or  $[L_w(\lambda)]_N$  are needed for such algorithms that are not just ratios. In compliance with these requirements, the normalized water-leaving radiances at five wavelengths in the visible are among the geophysical products to be delivered routinely from SeaWiFS data.

Retrieving  $R(\theta_0)$  from the slant radiances  $L_w(\theta, \theta_0, \Delta\phi)$  requires knowledge of  $Q(\theta', \theta_0, \Delta\phi, \lambda, \text{Chl})$  to solve Eq. (6). Then  $R_0$  can be derived from  $R(\theta_0)$  by using the ratio  $f(0)/f(\theta_0)$ . Retrieving  $(L_w)_N$  similarly requires knowledge of  $Q_0(\lambda, \text{Chl})/Q(\theta', \theta_0, \Delta\phi, \lambda, \text{Chl})$  and of  $f(\theta_0)/f(0)$  to solve Eq. (8). Because the angular dependencies that are to be removed differ for different pigment concentrations, this concentration must be estimated first. Accordingly one must resort to the previously described iterative scheme before being able to produce normalized quantities. This is made clear by the following simulation (Fig. 8)

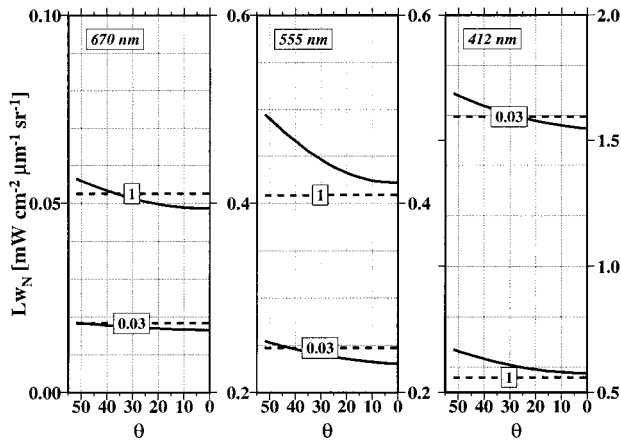


Fig. 8. Water-leaving radiances at all wavelengths have been computed in the same geometric conditions as for Fig. 7. Only three wavelengths and half of the swaths are displayed. These actual radiances are transformed into operational normalized water-leaving radiances [Appendix A, Eq. (A2)] and are shown as solid curves. They are also transformed into exact normalized water-leaving radiances (dashed lines) by way of Eq. (8) and by using the  $f/Q$  table after the chlorophyll concentration has been iteratively estimated (see text).

that was initiated in the same way as that above. With a given Chl value of 0.03 or 1  $\text{mg m}^{-3}$ , we can compute the corresponding  $L_w(\theta, \theta_0, \Delta\phi, \lambda, \text{Chl})$ . These water-leaving radiances regularly vary throughout the swath with higher values near the edge. If these  $L_w$ 's are transformed [according to Eq. (A2)] into operational normalized water-leaving radiances, the angular variations are kept practically unchanged (Fig. 8) because the solar angle  $\theta_0$  is almost constant along the scan line. Therefore such normalized radiances that still depend on the viewing geometry are not the meaningful quantities. Only the exact normalized water-leaving radiances, as well as  $R_0$ , are the unambiguous descriptors of the bio-optical state of the water.

When we start the process of transforming the measured  $L_w$ 's into exact  $(L_w)_N$  [Eq. (8)], the pigment content is still unknown. Accordingly the processing simulation consists of ignoring the Chl value used when we generated the signals and conversely of retrieving Chl through the iterative method previously described (with  $\lambda_1 = 443 \text{ nm}$  and  $\lambda_2 = 550 \text{ nm}$ ). Once Chl is known, the appropriate  $Q$  and  $f$  values for any wavelength can be selected in a lookup table in order to invert Eq. (8) and produce the exact water-leaving normalized radiances.

#### G. Sensitivity of the Bidirectional Reflectance to Wind Speed and Atmospheric Turbidity

With respect to the standard  $\tau_a$  value, i.e., 0.2 at 550 nm, the total aerosol content has been halved or doubled without changing its nature and relative vertical distribution. From zero, the wind speed has also been increased to 5 and 10  $\text{ms}^{-1}$ . The computations with these modified inputs have not been made in a systematic way, because we soon realized that their

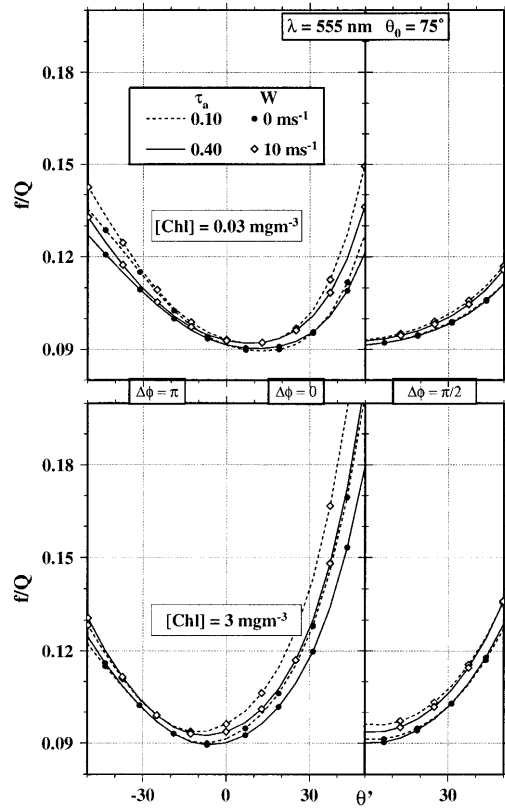


Fig. 9. Same as Fig. 6 (for  $\theta_0 = 75^\circ$  and  $\lambda = 555 \text{ nm}$ ) and for two other aerosol optical thicknesses (dashed and solid curves, respectively) and for two extreme values of the wind speed (filled and open symbols, respectively, for identification).

influence on the  $f/Q$  values are minor. Their effect is expected to be maximum when the amplitude in  $f/Q$  variations is at its maximum, namely, for large Sun angles and high chlorophyll concentrations. Selected examples in Fig. 9 demonstrate that, even when maximal, the changes in  $f/Q$  do not exceed 10%. We have determined that, with lower  $\theta_0$  values, the changes are almost undetectable except near the edges when  $\theta' > 30^\circ$ . As a consequence, the influence of these parameters can be safely neglected and a single table for the  $f/Q$  values appears to be sufficient (corrections, if really needed, could be prepared for exceptional situations).

## 6. Conclusions

Extracting from remotely sensed marine radiances any radiometric quantity that is free from angular dependencies and is thus truly fundamental is not a straightforward process. The complexity, however, is not unexpected. In the early era of ocean color interpretation and application, the natural inclination was to confound the apparent and inherent optical properties for a preliminary and simplified approach. Indeed, as soon as  $f$  and  $Q$  are considered constant, apparent quantities such as  $R$  or  $(L_w)_N$  *de facto* (and erroneously) become inherent properties (as being related only to  $b_b$  and  $a$ ). The second step, based on the full radiative transfer equation, restores these radio-

metric quantities to their status of apparent properties at the cost of some additional computations.

From a practical viewpoint, such computations are not cumbersome to the extent that precomputed  $f/Q$  values can be tabulated and then easily used in iterative procedures. At this point it is worth noting that these tables and their validity rely on a bio-optical model that applies only to case 1 waters and chlorophyll concentrations less than approximately  $3 \text{ mg m}^{-3}$ . The  $f/Q$  lookup tables that are currently available are not seen as a final answer. With a better knowledge of the VSF for various components that form the oceanic hydrosols,<sup>13,29</sup> improvements and extension toward higher Chl values are possible and desirable. Stokes vector computation of the upward radiance<sup>30</sup> could be envisaged; it is likely premature, considering the inaccuracies that remain in the current bio-optical models. In this study, the particular case of coccolithophore blooms is not considered. In this case, as in turbid, sediment-dominated, case 2 waters, the role of molecular scattering becomes vanishingly small. By analogy with case 1 waters with high Chl (Fig. 6), it can be anticipated that the amplitude of the  $f/Q$  variations could be large. This amplitude, however, is regulated by the shape of the VSF, and the VSF for liths or sediments is likely to differ from that adopted in the current bio-optical model. Thus specific computations are needed.

Because the chlorophyll concentration is one of the entries for the  $f/Q$  lookup table, this quantity must be estimated first. Such a requirement actually modifies the commonly accepted views relative to the ocean color processing. It was generally envisaged to process the marine signals, in terms of reflectances or normalized water-leaving radiances, before entering into any algorithm. According to our study, it appears necessary to identify the bio-optical state of the water body first, which can be conveniently described by Chl (used as an index) before any  $R(\lambda)$  or  $[L_w(\lambda)]_N$  can be derived. Because the derivation of Chl is based on a simple ratio technique, it is only weakly affected by the angular effect issues (even before iterations). Indeed, only the difference in the bidirectional behavior of the radiances at two wavelengths is involved. For each wavelength considered separately, this advantage cancels out. In this case the full impact of the bidirectional character of the upward radiance field has to be faced to produce absolute values for  $R(\lambda)$  and  $[L_w(\lambda)]_N$  as required by various algorithms based on sums, differences, or other combinations of radiometric quantities.

## Appendix A

The initial operational definition<sup>4</sup> of the normalized water-leaving radiance indicates the need for transforming any water-leaving radiance into a more fundamental quantity, insofar as the influence of the atmosphere and the solar zenith angle could be removed. The status of the vertically emerging radiance, as measured in field experiments, and that of a water-leaving radiance, as derived from space obser-

vation, actually differ as soon as the bidirectional effects are properly accounted for. For the former and following the recently recommended protocols for SeaWiFS validation,<sup>31</sup> the measured radiometric quantity is  $L_w(\theta' = 0, \theta_0)$ , the nadir radiance at null depth; then it is propagated upward through the sea surface [with Eq. (1)] to derive  $L_w(\theta = 0, \theta_0)$ . Finally this radiance is transformed into an operational normalized water-leaving radiance through

$$[L_w]_N^f = \frac{L_w(\theta = 0, \theta_0)}{\epsilon t(\theta_0) \cos \theta_0}, \quad (\text{A1})$$

where superscript  $f$  represents the field measurements. The presence of  $\cos \theta_0$  confirms the fact that the Sun is not at the zenith when the measurement is made. This definition, however, ignores the dependence of nadir radiance on the Sun position ( $\theta_0$ ). It was correct, i.e., coinciding with the exact definition leading to Eq. (7) now denoted  $(L_w)_N^{\text{ex}}$  (superscript ex for exact), as long as  $Q$  was believed to be constant. Actually  $L_w(0, \theta_0)$  involves the specific factor for nadir viewing measurement  $Q_n(\theta_0)$  [expression (9b)] that undergoes considerable variations with  $\theta_0$  (Figs. 3 and Fig. 4). This issue certainly requires that more attention be paid to calibration-validation experiments in support of ocean color sensors and when protocols are recommended. It is worth noting that the  $Q_n$  variations also depend on pigment content and wavelength.

When we transcribe the water-leaving radiances that are observed from space into a normalized radiance, the dependence on  $\theta_0$  subsists as above. A second angular effect is added because the viewing angle now varies within the swath (see Fig. 8). A simple transformation of  $L_w(\theta, \theta_0, \Delta\phi)$ , as suggested by Eq. (A1), provides (superscript  $s$  represents space measurements)

$$(L_w)_N^s = \frac{L_w(\theta, \theta_0, \Delta\phi)}{\epsilon t(\theta_0) \cos \theta_0}. \quad (\text{A2})$$

This quantity strictly coincides with  $(L_w)_N^f$  only when  $\theta = 0$ . So the two above normalized quantities, expected to be fundamental and strictly comparable, are not accurately defined as they are not equal and still varying.

It is necessary to resort to  $(L_w)_N^{\text{ex}}$ , which (like  $R$ ) is unambiguous. The relationships between the three normalized radiances can be straightforwardly derived from Eqs. (7) and (8) and are as follows:

$$\begin{aligned} (L_w)_N^{\text{ex}} &= \frac{\Re_0}{\Re(\theta)} \frac{R_0}{R(\theta_0)} \frac{Q(\theta', \theta_0, \Delta\phi)}{Q_0} (L_w)_N^s \\ &= \frac{R_0}{R(\theta_0)} \frac{Q_n(\theta_0)}{Q_0} (L_w)_N^f. \end{aligned} \quad (\text{A3})$$

Note that according to Eq. (10a) the ratio  $R_0/R(\theta_0)$  has to be replaced by the ratio  $f(\theta_0 = 0)/f(\theta_0)$ .

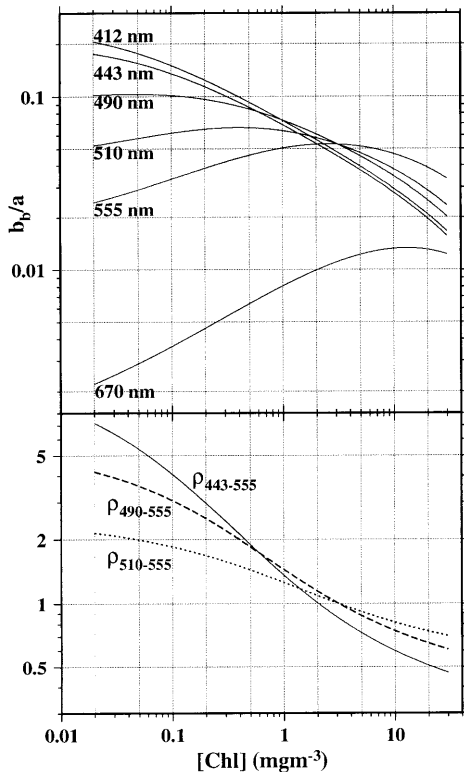


Fig. 10. Variations of  $b_b/a$  as a function of Chl for various wavelengths, and of some of their ratios, based on the bio-optical model summarized in Appendix C.

### Appendix B

As above, the Sun is not necessarily at the zenith when we derive the RS reflectance is derived from measured nadir radiance, so that

$$R_{RS} = \frac{L_w(\theta = 0, \theta_0)}{E_d(0^+, \theta_0)}$$

According to Eq. (5b) this RS reflectance corresponds to

$$R_{RS} = \frac{\mathfrak{R}_0}{Q_n(\theta_0)} R = \frac{(L_w)_N f}{F_0}$$

or also [Appendix A, Eq. (A3)]

$$R_{RS} = (L_w)_N^{\text{ex}} \frac{Q_0}{Q_n(\theta_0)} \frac{R(\theta_0)}{R_0} \frac{1}{F_0}$$

This quantity, although not discussed in this paper, can be introduced into the expressions giving the bidirectional radiances by using the above equivalences. Note that another remotely sensed reflectance has also been defined<sup>32</sup> that uses the scalar downwelling irradiance rather than the plane downward irradiance. Similar expressions as those above can be derived.

### Appendix C

It is outside the scope of this paper to discuss or advocate any particular model for retrieving various

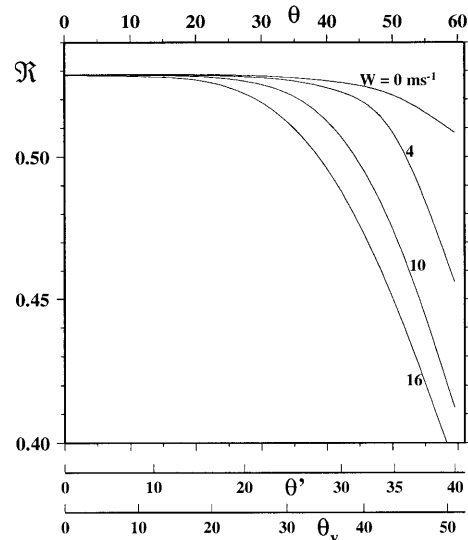


Fig. 11. Variations of  $\mathfrak{R}(\theta)$ , a term that merges all the reflection and refraction effects [Eq. (5)], with  $\theta$  and for several wind speeds as indicated. In correspondence with the  $\theta$  scale the  $\theta'$  and  $\theta_v$  scales are also given ( $\theta_v$  is the viewing angle from a satellite at an altitude of 705 km).

optically active substances (see, e.g., Refs. 11, 27 and 28) from the data to be delivered by future sensors. A model however is currently needed when one examines the possibility of operating iterative techniques with the aim of circumventing the bidirectional effects. This model must allow the signals (the  $L_w$ 's) to be simulated for all pixels within a scan line; hereafter it will be used again (in its reverse form) to process the signals iteratively. In such a numerical demonstration of the efficiency of removing the angular effects, the choice of model does not actually matter.

The bio-optical model currently used deals only with case 1 waters and only with one constituent, that is Chl, even if this single denomination<sup>18</sup> covers a complex combination of phytoplankton, bacteria, detritus, etc. What we really need is an index that can be used to identify the water body. Such an identification could rely on the reflectance model (Fig. 13 in Ref. 17), where  $f$  [in Eq. (10a)] was given a unique value (0.33) and absorption coefficient  $a$  was progressively derived from  $K_d$ . If we take into consideration that  $f$  may undergo considerable variations (Fig. 2), it seems wiser to disregard the above constant value. Therefore the concept of a reflectance model can be abandoned and replaced by a bio-optical model restricted to linking the variations of  $b_b(\lambda)/a(\lambda)$  with those of Chl. Examples are provided in Fig. 10, together with the variations of several ratios including the so-called blue-to-green ratio expressed by

$$\rho_{443-555} = \frac{\alpha(443)b_b(555)}{\alpha(555)b_b(443)}$$

The corresponding polynomial fit (better than 1%) to this curve, which is used as an algorithm for the

retrieval of Chl, is

$$Y = \sum_{n=0}^5 A_n X^n,$$

where  $Y = \ln [\text{Chl}]$  and  $X = \ln \rho$  and the coefficients are

$$A_0 = 0.71576, \quad A_1 = -2.48781, \quad A_2 = 0.71844, \\ A_3 = -0.60042, \quad A_4 = 0.29756, \quad A_5 = -0.08105.$$

The reproduction of the curve remains accurate (within  $\pm 3\%$ ) with a polynomial fit limited to the third degree. Similar curves and polynomials are available for other pairs of wavelengths (e.g., 490–555 or 510–555 nm).

#### Appendix D

Variations of the reflection–refraction term  $\mathfrak{R}(\theta)$  can be found in Refs. 9, 33, and 34. For the sake of completeness, they are summarized below.

The transmission of the sea surface for sky and Sun irradiance expressed by  $(1 - \bar{\rho})$  is equal to 0.957 ( $\pm 3\%$  according to atmospheric turbidity and Sun elevation). The internal reflectance, accounted for by  $(1 - \bar{r}R)$ , where  $\bar{r}$  is 0.489, varies slightly with  $R$ . With a mean  $R$  value of 3% this term is equal to 0.985 ( $\pm 1.5\%$ ) if  $R$  varies between 0 and 6%. We can safely assume that these two terms are constant, as well as  $n^{-2}$  ( $= 0.556$ ). The main variations of  $\mathfrak{R}(\theta)$  result only from the Fresnel downward reflection that affects the upwelled radiance before emergence and reads  $[1 - \rho(\theta', \theta)]$ . If we consider only the remote-sensing configuration, this transmittance term, for a perfectly flat sea, varies from 0.979 ( $\theta = 0$ ) to as low as 0.939 ( $\theta = 60^\circ$ , leading to  $\theta' \approx 40^\circ$ ). This range of variations, however, increases considerably for a rough sea and can be related to the wind speed as tabulated in Ref. 9 and displayed in Fig. 11. The  $\mathfrak{R}$  value for  $\theta = 0$ , which is practically insensitive to wind speed, amounts to 0.529.

We are pleased to acknowledge support for this study from European Space Telecommunication (ESTEC) and the European Space Agency (ESA) under contracts ESA-ESTEC OT/MM/612 and ESA 11345/95/NL-PR. We are indebted to H. R. Gordon and an anonymous reviewer for their helpful suggestions and comments, and to C. D. Mobley for providing the possibility of checking our initial computations by using the HYDROLIGHT 3.0 code.

#### References and Notes

1. A. Morel and B. Gentili, "Diffuse reflectance of oceanic waters. II. Bidirectional aspects," *Appl. Opt.* **32**, 6864–6879 (1993).
2. A. Morel, K. J. Voss, and B. Gentili, "Bidirectional reflectance of oceanic waters: a comparison of modeled and measured upward radiance fields," *J. Geophys. Res.* **100**, 13,143–13,151 (1995).
3. K. J. Voss, "Electro-optic camera system for measurement of the underwater radiance distribution," *Opt. Eng.* **28**, 241–247 (1989).
4. H. R. Gordon and D. K. Clark, "Clear water radiances for atmospheric correction of Coastal Zone Color Scanner imagery," *Appl. Opt.* **20**, 4175–4180 (1981).
5. A. Bricaud and A. Morel, "Atmospheric corrections and interpretation of marine radiances in CZCS imagery: use of a reflectance model," *Oceanol. Acta* **7**, 33–50 (1987).
6. J. M. André and A. Morel, "Atmospheric corrections and interpretation of marine radiances in CZCS imagery, revisited," *Oceanol. Acta* **14**, 3–22 (1991).
7. C. Myrmehl and A. Morel, "Accounting for the marine reflectance bidirectionality when processing remotely sensed ocean colour data," in *Ocean Optics XII*, J. S. Jaffe, ed., Proc. SPIE **2258**, 870–878 (1994).
8. H. R. Gordon and A. Morel, "Remote assessment of ocean color for interpretation of satellite visible imagery," in *Lecture Notes on Coastal and Estuarine Studies*, R. T. Barber, C. N. K. Mooers, M. J. Bowman, and B. Zeitzschel, eds., (Springer-Verlag, Berlin, 1983), Vol. 4.
9. R. W. Austin, "The remote sensing of spectral radiance from below the ocean surface," in *Optical Aspects of Oceanography*, N. G. Jerlov and E. S. Nielsen, eds. (Academic, San Diego, Calif., 317–344 (1974).
10. K. L. Carder and R. G. Steward, "A remote sensing reflectance model of a red tide dinoflagellate off West Florida," *Limnol. Oceanogr.* **30**, 286–298 (1985).
11. Z. P. Lee, K. L. Carder, S. K. Hawes, R. G. Steward, T. G. Peacock, and C. O. Davis, "Model for the interpretation of hyperspectral remote-sensing reflectance," *Appl. Opt.* **33**, 5721–5732 (1994).
12. A. Morel and B. Gentili, "Diffuse reflectance of oceanic waters: its dependence on Sun angle as influenced by the molecular scattering contribution," *Appl. Opt.* **30**, 4427–4438 (1991).
13. As discussed in Refs. 1 and 12, the unique nature of the VSF for particles limits the validity of the modeled inherent optical properties. With this VSF, when the chlorophyll levels are above  $1.5 \text{ mg m}^{-3}$ , the backscattering efficiency becomes too high and contradicts the empirical relationship providing the backscatter coefficient as a function of Chl proposed in Ref. 18. Therefore, above this limit, results become dubious. Attempts to model the VSF of marine hydrosols from the VSF of several constituents already exist,<sup>28</sup> even if data for these VSF's and their respective roles are currently scarce.
14. A. Morel and L. Prieur, "Analysis of variations in ocean color," *Limnol. Oceanogr.* **22**, 709–722 (1977).
15. H. R. Gordon, O. B. Brown, and M. M. Jacobs, "Computed relationships between the inherent and apparent optical properties of a flat homogeneous ocean," *Appl. Opt.* **14**, 417–427 (1975).
16. A. Morel and H. R. Gordon, "Report of the working group on water color," *Boundary-Layer Meteorol.* **18**, 343–355 (1980).
17. A. Morel, "Optical modeling of the upper ocean in relation to its biogenous matter content (Case 1 waters)," *J. Geophys. Res.* **93**, 10,749–10,768 (1988).
18. The historical bio-optical algorithms that were developed during the CZCS era used the symbol C to designate the algal pigment concentration; C was supposed to be the sum of chlorophyll *a* and pheophytin *a*, as was determined by using the fluorometric method. It is now acknowledged that, because of the interference with Chl *b*, phaeopigments have been seriously overestimated. Therefore it is wise to return to the notation Chl, which also has the advantage of avoiding any confusion with the symbol C, for carbon, in papers in which both are involved.
19. C. D. Mobley, B. Gentili, H. R. Gordon, Z. Jin, G. W. Kattawar, A. Morel, P. Reinersman, K. Stamnes, and R. H. Stavn, "Comparison of numerical models for computing underwater light fields," *Appl. Opt.* **32**, 7484–7504 (1993).
20. L. Elterman, "UV, visible, and IR attenuation for altitudes to 50 km," Environmental Research Paper 285, AFCRL-68-0153.

- (Air Force Cambridge Research Laboratories, Bedford, Mass., 1968).
21. E. P. Shettle and R. W. Fenn, "Models for the aerosols of the lower atmosphere and the effects of humidity variations on their optical properties," Environmental Research Paper 676, AFGL-TR-79-0214. (Air Force Geophysics Laboratory, Hanscom Air Force Base, Mass., 1979).
  22. C. Cox and W. Munk, "Some problems in optical oceanography," *J. Mar. Res.* **14**, 63–78 (1955).
  23. C. D. Mobley, *Light and Water: Radiative Transfer in Natural Waters* (Academic, San Diego, Calif., 1994), p. 592.
  24. J. T. O. Kirk, "Dependence of the relationship between inherent and apparent optical properties of water on solar altitude," *Limnol. Oceanogr.* **29**, 350–356 (1984).
  25. H. R. Gordon, "Dependence of the diffuse reflectance of natural waters on the sun angle," *Limnol. Oceanogr.* **34**, 1484–1489 (1989).
  26. W. W. Gregg, F. S. Platt, and R. H. Woodward, "The simulated SeaWiFS data set, Version 2," S. B. Hooker and E. R. Firestone, eds., Vol. 15 of NASA Tech. Memo. 104566 (1994), pp. 1–42.
  27. K. L. Carder, S. K. Hawes, K. A. Baker, R. C. Smith, R. G. Steward, and B. G. Mitchell, "Reflectance model for quantifying chlorophyll *a* in presence of productivity degradation products," *J. Geophys. Res.* **96**, 20,599–20,611 (1991).
  28. S. Sathyendranath, F. E. Hoge, T. Platt, and R. N. Swift, "Detection of phytoplankton pigments from ocean color: improved algorithms," *Appl. Opt.* **33**, 1081–1089 (1994).
  29. A. D. Weidemann, R. H. Stavn, J. R. V. Zaneveld, and M. R. Wilcox, "Error in predicting hydrosol backscattering from remotely sensed reflectance," *J. Geophys. Res.* **100**(C7), 13,163–13,177 (1991).
  30. G. W. Kattawar and C. N. Adams, "Stokes vector calculations of the submarine light field in an atmosphere-ocean with scattering according to a Rayleigh phase matrix: effect of interface refractive index on radiance and polarization," *Limnol. Oceanogr.* **34**, 1453–1472 (1989).
  31. J. L. Mueller and R. W. Austin, "Ocean optics protocols for SeaWiFS validation, Revision 1," S. B. Hooker, E. R. Firestone, and J. G. Acker, eds., Vol. 25 of NASA Tech. Memo. 104566 (1995), pp. 1–67.
  32. J. R. V. Zaneveld, "A theoretical derivation of the dependence of the remotely sensed reflectance of the ocean on the inherent optical properties," *J. Geophys. Res.* **100**(C7), 13,135–13,142 (1991).
  33. H. R. Gordon, O. B. Brown, R. H. Evans, J. W. Brown, R. C. Smith, K. S. Baker, and D. K. Clark, "A semianalytic radiance model of ocean color," *J. Geophys. Res.* **93**, 10,909–10,924 (1988).
  34. A. Morel and D. Antoine, "Heating rate within the upper ocean in relation to its bio-optical state," *J. Phys. Oceanogr.* **24**, 1652–1665 (1994).